PERIODICO di MINERALOGIA
established in 1930

DIPARTIMENTO
DI SCIENZE DELLA TERRA

SAPIENZA
UNIVERSITÀ DI ROMA

An International Journal of
Mineralogy, Crystallography, Geochemistry,
Ore Deposits, Petrology, Volcanology
and applied topics on Environment, Archaeometry and Cultural Heritage

Anomalous chromite-ilmenite parageneses in the Chapesvara and Lyavaraka ultramafic complexes, Kola Peninsula, Russia

Andrei Y. Barkov [1,*], Andrey A. Nikiforov [1], Vladimir N. Korolyuk [2], Larisa P. Barkova [1], Robert F. Martin [3]

[1] Research Laboratory of Industrial and Ore Mineralogy, Cherepovets State University, 5 Lunacharsky Avenue, 162600 Cherepovets, Russia
[2] V.S. Sobolev Institute of Geology and Mineralogy, Siberian Branch of the Russian Academy of Science, 3 Avenue "Prospekt Koptyuga", 630090 Novosibirsk, Russia
[3] Department of Earth and Planetary Sciences, McGill University, 3450 University Street, Montreal, Quebec H3A 0E8, Canada

ARTICLE INFO

Submitted: April 2020
Accepted: June 2020
Available on line: September 2020

* Corresponding author:
ore-minerals@mail.ru

DOI: 10.2451/2020PM16622

How to cite this article:
Barkov A.Y. et al. (2020)
Period. Mineral. 89, 299-317

ABSTRACT

The Serpentinite Belt of the Kola Peninsula, Russia, contains a string of dislocated bodies of fairly fresh to variously serpentinized dunite, harzburgite and orthopyroxenite. We focus here on the association of chromian spinel and ilmenite in the Chapesvara-I and -II ultramafic bodies, which occur close to the Pados-Tundra layered complex. On the basis of the mineral compositions obtained, Chapesvara-I and -II belong to a single complex that crystallized in a subvolcanic setting. The first generation of chromite is relatively enriched in Mg and Zn in its core, and is free of inclusions. Oddly, zinc and manganese are decoupled, and Mn shows the expected rimward increase. The second generation of chromite is relatively poor in Mg and full of included clinochlore, interpreted to have crystallized from trapped aqueous fluid, similar to clinochlore in the laurite-clinochlore intergrowths hosted by grains of magnesiochromite-chromite at Pados-Tundra. The late buildup in the geikielite component of ilmenite, documented in both the Chapesvara and Lyavaraka complexes, is attributed to the progressive buildup of oxygen in the late melt owing to the preferential loss of hydrogen during crystallization.

Keywords: ultramafic rocks, komatiites; Cr-Ti mineralization; chromite-ilmenite association; zonation of chromian spinels; Chapesvara complex; Lyavaraka complex; Serpentinite Belt; Kola Peninsula; Russia.

INTRODUCTION

The Serpentinite Belt in the Kola Peninsula consists of northeasterly trending suites of ultramafic bodies of relatively unaltered bodies of dunite-harzburgite-orthopyroxenite and related foliated serpentinites (Shukevich, 1933, 1936; Murashov, 1958). The belt includes fragmented blocks displaced tectonically toward the northeast over a distance of ~25 km close to the border of Russia with Finland. The mineral assemblages in these ultramafic bodies indicate a high level of oxygen fugacity (fO_2), in general, and the rocks appear to have crystallized in a subvolcanic environment. In this paper, we describe 1) the resulting unusual characteristics of the chromite-ilmenite assemblages in two important complexes, Chapesvara and Lyavaraka, 2) two generations of chromian spinel at Chapesvara, and 3) the contrasting behavior of the minor elements Zn and Mn, as revealed in terms of patterns of zonation.

Geological setting and samples

The Pados-Tundra layered complex, exposed over 6 km, is the largest member of the Serpentinite Belt;

it hosts stratiform and podiform chromitite deposits mineralized in the platinum-group elements (Mamontov and Dokuchaeva, 2005; Barkov et al., 2016, 2017a, 2017b). The Chapesvara-I and Chapesvara-II bodies also contain disseminated chromite, associated with ilmenite. These bodies typically represent differentiated sills of a subvolcanic nature. Chapesvara-II has a well-developed core of dunite (Barkov et al., 2019). Ultramafic bodies of the Serpentinite Belt include the Kareka-Tundra suite in the west, the Mount Khanlauta suite close to Pados-Tundra, and the Lotmvara (I and II) bodies in the eastern portion of the region. The Lyavaraka complex (Khlebnaya varaka) is located in the River Pecha basin area ~65 km northeast of the Chapesvara-II body (Figure 1 a,b). It also consists of dunite-harzburgite-orthopyroxenite sequences (Spirov, 1972; Dokuchaeva, 1981). In the opinion of Vinogradov (1971), the overall extent of the Serpentinite Belt could even exceed 200 km along a curved boundary, to the southwestern end of the Sal'nie Tundry area.

The ultramafic intrusive bodies making up the Serpentinite Belt are closely associated with major shear zones accompanied by a collisional mélange developed

Figure 1 (a, b). Location map of the Chapesvara-I, Chapesvara-II and Lyavaraka complexes (a) and the sample location at Lyavaraka shown in the SAS Planet image (b).

as a part of the Tanaelv high-grade ductile thrust belt. They are positioned along the curved boundary of the two large terranes of the Baltic Shield: the Paleoproterozoic Lapland Granulite Terrane, LGT (or Lapland Granulite Belt), forming part of the Paleoproterozoic Lapland-Kola Collisional Orogen (LKCO), and the Belomorian Composite Terrane (BCT) of Archean age (cf. Balagansky et al., 2016). These sill-like bodies likely formed by injection of a primitive komatiitic magma, derived from a common mantle source, along a subparallel system of north-northeast-trending regional shear zones (Barkov et al., 2019).

The Chapesvara-I and Chapesvara-II bodies are located close to the contact of two regional units composed of granite, granitic gneiss, migmatite and anatectic granodiorite, along with two-mica garnet-kyanite schist belonging to the Belomorian series (Figure 2 a-c). The Chapesvara-I body lies fairly close to the Pados-Tundra layered complex and is located about 8 km southwest of Chapesvara-II. The Chapesvara-I body was presumably dislocated during the Paleoproterozoic orogeny. As a result, most exposures examined (Figure 2a) consist of blocks ≤1 to 3-4 m across. Chapesvara-II is among the largest and better-preserved bodies of the Serpentinite Belt. It was investigated along a traverse oriented across the sill-like body (Figure 2b). Representative specimens were taken along the entire cross-section. These define the following units (bottom to top): Amphibole-olivine zone (IV), Central dunite zone (II), Olivine-bearing orthopyroxenite zone (III), and the Upper contact facies (I). These lithologies represent a comagmatic series formed in the order from I to IV under closed-system conditions during crystallization of a komatiitic magma. The zone of high-MgO dunitic rocks crystallized *in situ* in the central portion of the sill. Crystallization proceeded along two fronts, moving upward and downward, respectively (Barkov et al., 2019). In spite of the influence of tectonic processes, the bulk composition of most of the fifty samples collected at Chapesvara-I and Chapesvara-II remained virtually unaltered. The primary associations of rock-forming and accessory minerals are well preserved, with only minor extents of deuteric alteration (i.e., serpentine, clinochlore, talc, secondary amphiboles and a Mg-rich carbonate).

The Lyavaraka intrusion is close to being isometric in shape (Figure 3). It is dominantly composed of orthopyroxenite, the "bronzitite" of previous investigators (Spirov, 1972). More magnesian varieties of orthopyroxenite, or "enstatitite", occur as pegmatitic rocks located mostly at the northern contact of the body, and as internal zones interpreted to be due to a local enrichment in a fluid phase. The most prominent characteristic is the development of a highly magnesian core mapped in

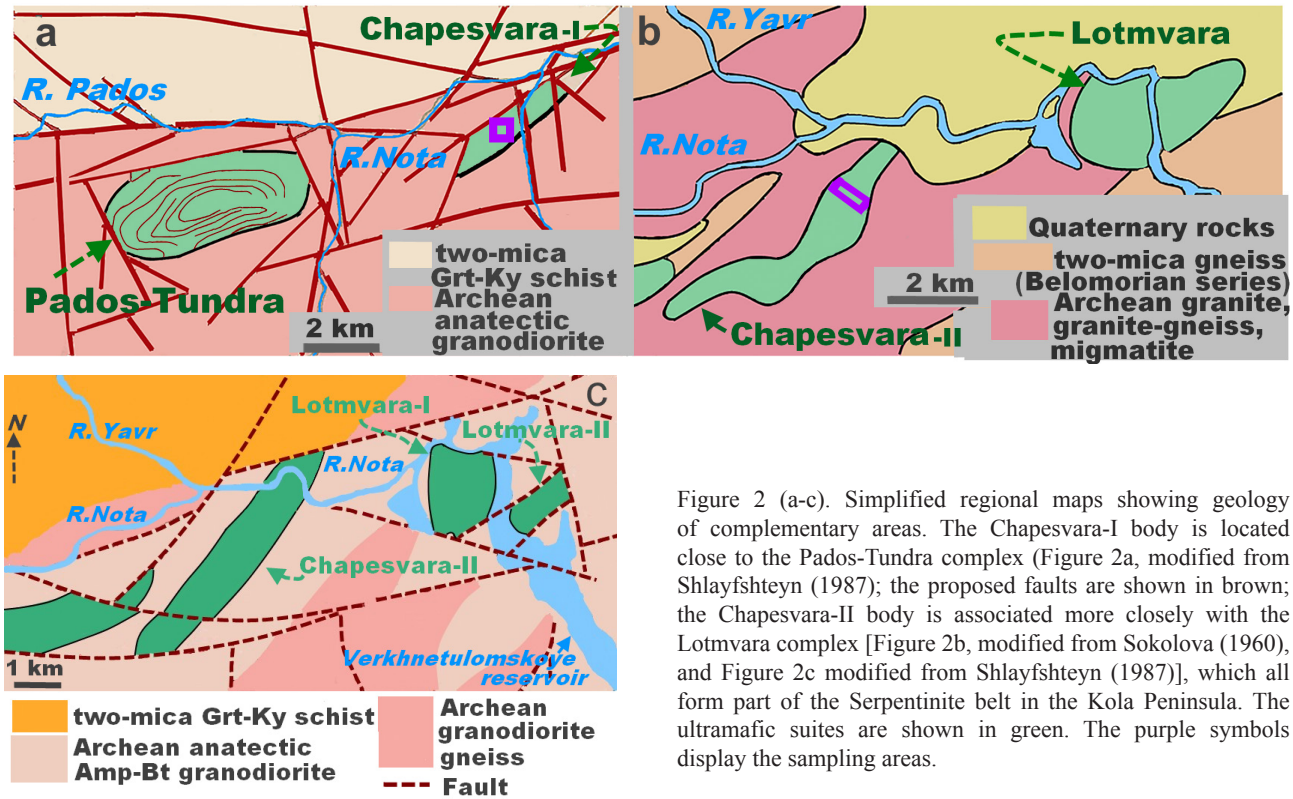

Figure 2 (a-c). Simplified regional maps showing geology of complementary areas. The Chapesvara-I body is located close to the Pados-Tundra complex (Figure 2a, modified from Shlayfshteyn (1987); the proposed faults are shown in brown; the Chapesvara-II body is associated more closely with the Lotmvara complex [Figure 2b, modified from Sokolova (1960), and Figure 2c modified from Shlayfshteyn (1987)], which all form part of the Serpentinite belt in the Kola Peninsula. The ultramafic suites are shown in green. The purple symbols display the sampling areas.

the southern portion of the complex. Most of the olivine accumulated to the core, along with the associated "enstatitite" and minor chromitite (Figure 3). A trachytic texture is observed in some outcrops of orthopyroxenite. Variously textured varieties of two-amphibole (tremolite-actinolite series and anthophyllite) rocks, which commonly are pegmatitic, show intimate intergrowths of large grains of orthopyroxene with these amphiboles of late magmatic or deuteric origin. The analyzed sample LVR-37A is a pegmatitic orthopyroxene-two-amphibole rock, with orthopyroxene grains up to 5 cm across. We also observed a minor development of other orthopyroxene-dominant rocks containing subordinate amounts of clinopyroxene, plagioclase, magnesian mica, and minor quartz.

Analytical details

Electron-microprobe analyses were conducted at the Analytical Center for Multi-Elemental and Isotope Studies, Institute of Geology and Mineralogy, SB RAS, Novosibirsk, using a JEOL JXA-8100 instrument in wavelength-dispersion spectrometry mode (WDS). An accelerating voltage of 20 kV and a probe current of 50 nA were used for olivine, chromian spinel and ilmenite. We employed *K*α analytical lines for all elements except Cr, where the $K\beta_1$ line was used because of peak overlap. Periods of measurements at the peaks were 20 s. In the background position, measurements lasted 5 s on both sides of the line; for the V*K*α line, measurements lasted 10 s on the lower side of the analytical signal (crystal analyzer LiF, BG position -2 mm). The superposition of the Ti$K\beta_1$ line on the V*K*α line and of the V*K*β line on the Cr*K*α line were accommodated using the OVERLAP CORRECTION software. The beam diameter was 1-2 μm. Natural specimens of olivine (Mg, Si, Fe, and Ni) and chromiferous or manganiferous garnet (Ca, Cr and Mn) were used as standards for olivine. A natural specimen of magnesian chromite (for Cr, Fe, Mg, and Al), manganiferous garnet (Mn), ilmenite (Ti) and the synthetic oxides $NiFe_2O_4$ (Ni), $ZnFe_2O_4$ (Zn), and V_2O_5 (V) were used as standards for chromian spinel and ilmenite. The data were processed with the ZAF method of corrections. The calculated values of detection limit (1σ) are: 0.01 wt% for Cr and <0.01 wt% for Ni, Ca, Zn and Mn. The accuracy and reproducibility of the analytical procedures were evaluated with special tests (Korolyuk et al., 2009, Lavrent'ev et al., 2015).

Grains of coexisting chromite and ilmenite in samples taken from the Lyavaraka complex were chemically analyzed at the same analytical center with an INCA Energy 450+XMax 80 energy-dispersive spectrometer (EDS, Oxford Instruments Ltd.) used with a MIRA 3 LMU scanning electron microscope (SEM, Tescan Ltd.).

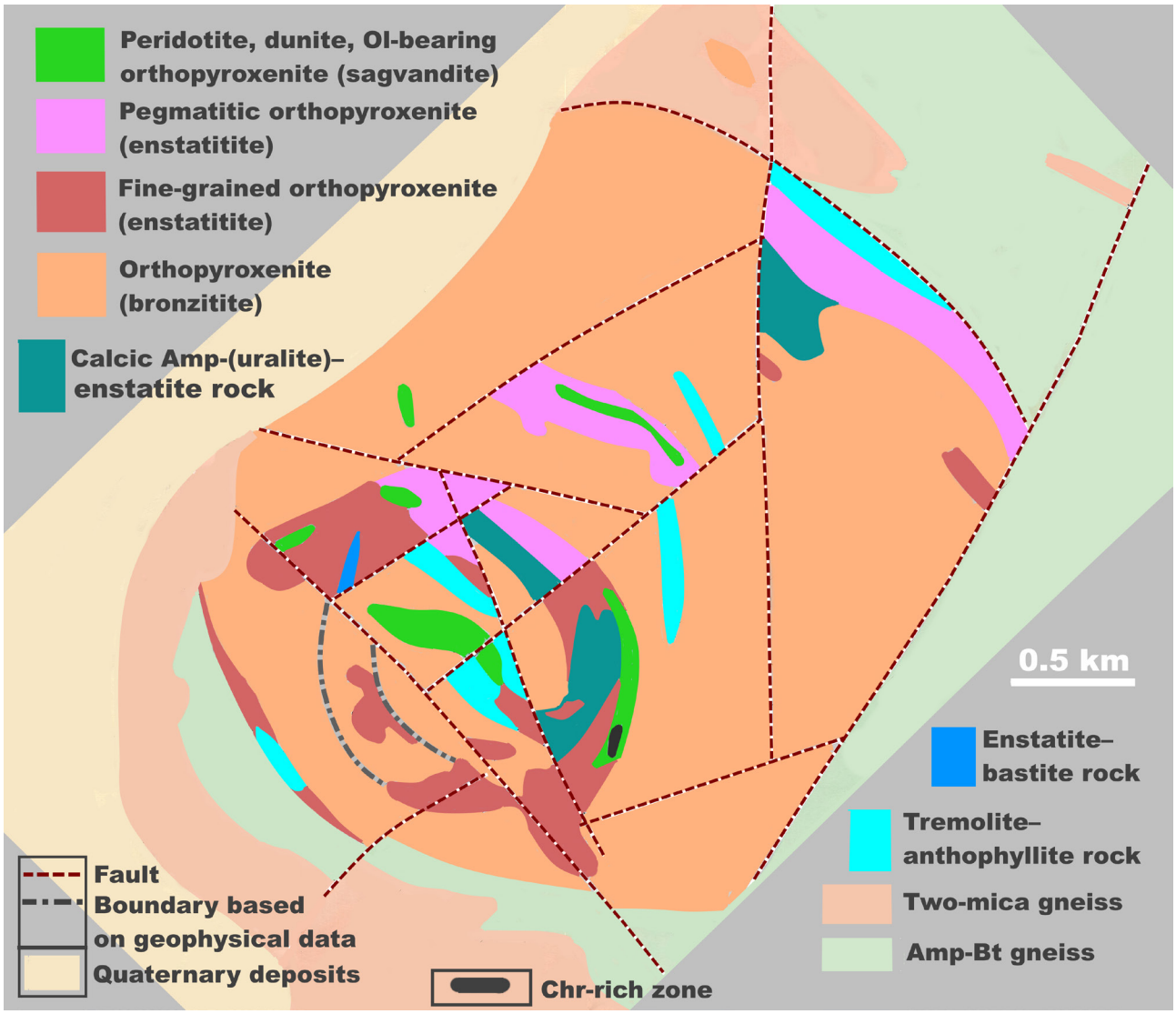

Figure 3. Geological map of the Lyavaraka complex, Kola Peninsula (after Spirov, 1972).

OUR RESULTS

Rock-forming silicates and chromite-ilmenite mineralization at Chapesvara

The ultramafic rocks of the Chapesvara-I and Chapesvara-II bodies are fairly similar. They correspond to dunite, harzburgite and olivine orthopyroxenite, all typically with a fine-grained texture (Figure 4 a,b). The ranges of bulk-rock concentrations of MgO (and SiO_2) established by XRF analyses (cf. Barkov et al., 2019) compare well: 28.2-41.63 (38.18-49.15) at Chapesvara-I *versus* 28.47-44.90 (38.2-52.97) wt% at Chapesvara-II. Interestingly, grains of a primary calcic amphibole (Amp) are present in association with olivine (Ol) and orthopyroxene (Opx), as observed in the Pados-Tundra complex; also, replacement relations involving Opx belonging to different generations are observed (cf. Barkov et al., 2017a). A directional texture, in which grains of Opx +Amp (±Ol) show a preferred orientation, is developed locally; spinifex textures were not encountered, however. In common with Pados-Tundra, the Ol-Opx association is characteristic of the entire Chapesvara complex. However, minor amounts of clinopyroxene (Cpx) and plagioclase (Pl) (both absent at Pados-Tundra) appear sporadically at Chapesvara-I and -II as reaction rims (Pl after Cpx and Amp after Pl). The observed associations of ore minerals include grains of chromian spinel, Mg-bearing ilmenite, and Co-bearing pentlandite, all of which also occur in the Pados-Tundra complex (Barkov et al., 2017a).

The chromite-ilmenite (Chr-Ilm) mineralization

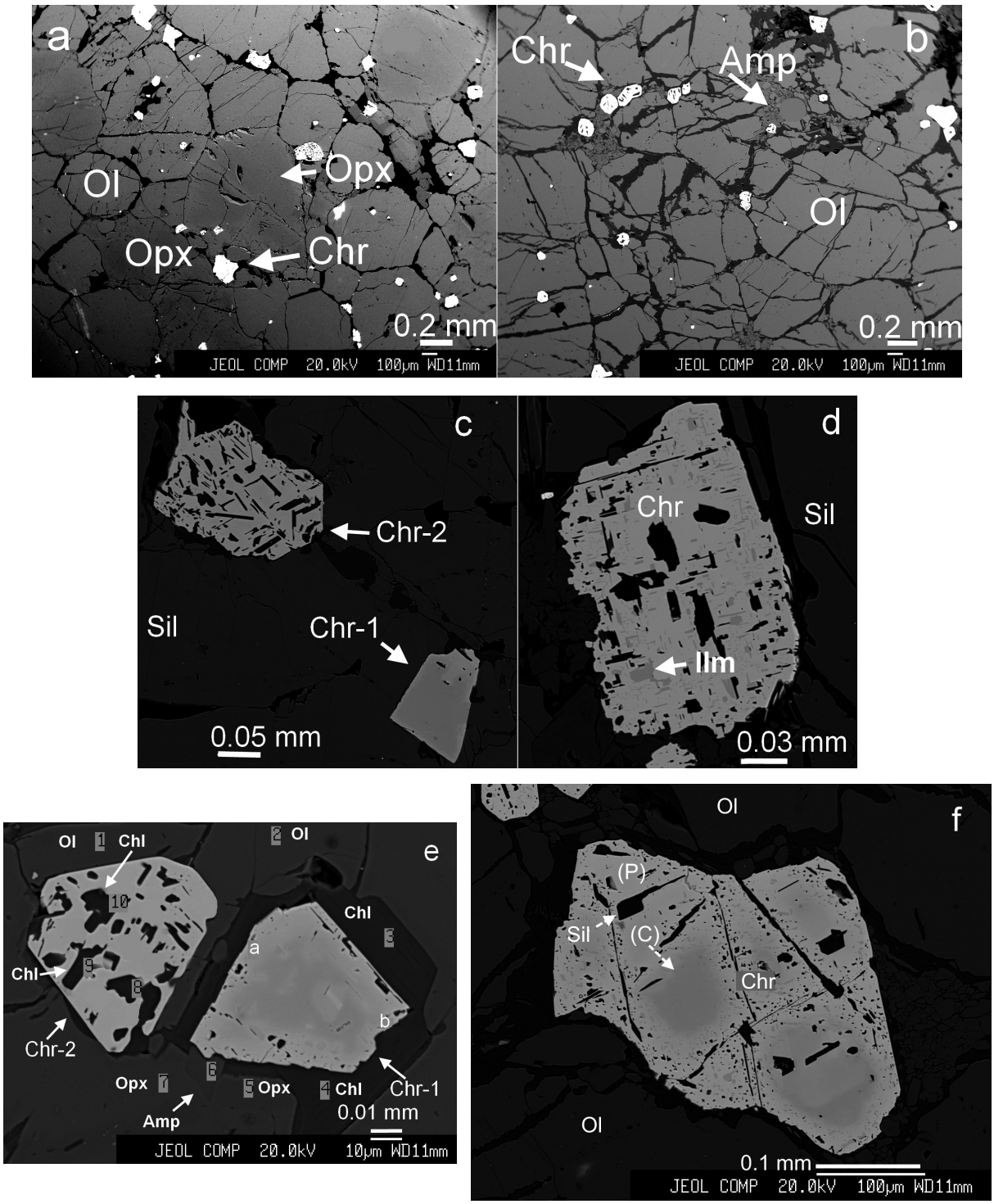

Figure 4 (a-f). BSE images showing characteristic textures of fine-grained ultramafic rocks at Chapesvara-I (Figure 4a) and Chapesvara-II (Figure 4b), grains of chromian spinel of the first (Chr-1) and second (Chr-2) generations hosted by a silicate mineral, Sil (Figure 4c), exsolution lamellae of ilmenite (Ilm) enclosed within the matrix of chromite, Chr (Figure 4d), and zoned grain of chromite (first generation: Chr-1) associated closely with another grain of chromite (second generation: Chr-2), which contains very abundant inclusions of clinochlore (Figure 4e). Numbers 1 to 10 pertain to points of WDS analyses presented in Table 1. Letters a and b (Figure 4e) show the path of detailed WDS traverse (ab), analytical results of which are shown in Tables 2, 3 and Figures 5 a-d. Figure 4f shows a zoned grain of chromian spinel (Chr), which consists of cores (C) and peripheral areas (P) (rich in inclusions of a silicate mineral, Sil, i.e., clinochlore),. It is associated with olivine ($Fo_{89.2-89.4}$) in a dunite in the Chapesvara-II sill (the sampling area is shown in Figure 2b).

at Chapesvara-I and -II occurs as heterogeneous disseminations of subhedral grains ≤0.2 mm across, typically located at boundaries of Ol and Opx grains (Figure 4 a,b). We distinguish two generations of chromian spinel. Grains of the first generation are essentially free of inclusions. In contrast, chromite grains of the second generation are exceptionally enriched in inclusions of clinochlore (Figure 4 c-e). Lamellae of the latter can exhibit a crystallographically controlled arrangement (Figure 4c). Ilmenite is markedly subordinate with respect to chromian spinel. It occurs as rare, separate and elongate grains ≤10-50 μm across defining a "printed circuit" pattern; the lamellae are possibly due to exsolution from the chromite host (Figure 4d).

Association, zonation and compositional variations of chromian spinel at Chapesvara

The pattern of zoning was investigated in a representative subhedral grain of first-generation chromite (Chr-1) closely associated with a subhedral grain of second-generation chromite (Chr-2: Figure 4e). Compositions of the coexisting silicates and hydrous silicates, the results of wavelength-dispersion analyses (WDS), are listed in Table 1. The location of point analyses #1 to 10 is shown in Figure 4e. The rest of the data-points (#11-18, Table 1) pertain to other grains analyzed in the same polished mount of harzburgite (sample CHP-7, Chapesvara-I). Grains of olivine are moderately highly magnesian in this sample: $Fo_{88.0\text{-}88.6}Fa_{10.9\text{-}11.5}Tep_{0.1\text{-}0.2}$ (Table 1, *n*=5). Close to a contact with chromite, the orthopyroxene (Figure 4e, #5) is somewhat richer in Mg than the other four grains analyzed: $En_{88.4}Fs_{11.5}Wo_{0.1}$ vs $En_{86.1\text{-}87.2}Fs_{10.0\text{-}11.4}Wo_{2.4\text{-}3.0}$; those are notably enriched in Cr: 0.61-0.69 wt% Cr_2O_3 (Table 1). Three grains of calcic amphibole correspond to tremolite:
$(Ca_{1.75\text{-}1.87}Na_{0.06\text{-}0.08})(Mg_{4.60\text{-}4.72}Fe_{0.23\text{-}0.26}Al_{0.08\text{-}0.19}Cr_{0.01\text{-}0.03}Mn_{0.01}Ti_{0.01})(Si_{7.98\text{-}8.01}Al_{0\text{-}0.02})O_{22}(OH)_2$.
They have high values of the Mg# index [100Mg/(Mg+Fe^{2+}+Mn)]: 94.5-95.4. The inclusions of clinochlore hosted by the grain of Chr-2 yield:
$(Mg_{4.66\text{-}4.75}Fe_{0.21\text{-}0.24}Ni_{0.01\text{-}0.02})Al(Si_{3.01\text{-}3.10}Al_{0.70\text{-}0.80}Cr_{0.16\text{-}0.23})O_{10}(OH)_8$; the Mg# value is in the range 95.0-95.8 (Figure 4e, Table 1).

The zoned grain of Chr-1 (Figure 4e) displays cryptic variations of composition measured along the *ab* traverse (#1-22, Tables 2, 3). Magnesium, Al and, surprisingly, Zn all covary, and show a gradual decrease in concentration from core to margin (Figures 5 a-d). The uniform behavior of Mg and Al reflects their incorporation as the spinel component. The observed levels of Fe in all its forms (i.e., total Fe, ferrous and ferric Fe), along with Mn, increase toward the margin (Figure 5 a-d). The high content of $Fe_2O_{3(calc)}$ attained at the margin, is noteworthy.

A closely associated pair of grains of Chr-1 (free of inclusions) and Chr-2 (rich in inclusions of clinochlore: Figure 4e) display striking differences of their compositions. The Chr-1 phase is substantially more magnesian and aluminous than Chr-2. As shown in Table 2 (#1-22 vs. #23-30), levels of MgO (and Al_2O_3) vary from 4.71 to 7.18 (10.57-20.43) vs. from 3.82 to 4.38 (5.79-7.0) wt%, respectively. In addition, the Chr-1 grain (first generation) is noticeably richer in Zn and poorer in Mn (Tables 2, 3) than Chr-2. The Chr-1 grain contains (WDS): MgO 5.40-7.75, Al_2O_3 13.67- 22.39, ZnO 0.38-0.47, MnO 0.40-0.47 wt%, with 26.0<Mg#<36.8 and 55.3<Cr#<69.4. The Chr-2 grain gave (WDS): MgO 4.37-5.33, Al_2O_3 8.94-12.84, ZnO 0.27-0.38, MnO 0.49-0.52 wt%, with 22.9<Mg#<26.7 and 72.1<Cr#<79.5 [Cr#=100Cr/(Cr+Al)]. The compositions of chromian spinel observed at Chapesvara-I and Chapesvara-II are similar; the same variation trends apply in diagrams Mg# vs. Cr# (Figure 6), Fe^{3+}# vs Mg# (Figure 7) [Fe^{3+}#=100Fe^{3+}/(Fe^{2+}+Fe^{3+})], and in the diagram Cr-Al-Fe^{3+} (Figure 8).

Mg/Fe values in coexisting chromite and ilmenite at Chapesvara

An anomalous distribution of values of the Mg/Fe ratio is documented in coexisting grains of chromite and ilmenite. Our compositional data (Table 4, Figure 9) indicate that the ilmenite grains (both the potential exsolution lamellae and discrete grains) invariably display a relative enrichment in Mg in comparison with the intimately associated chromite. The content of MgO and value of Mg# attain 5.8 wt% and 20.8 in the ilmenite grains, respectively. The ilmenite is thus significantly enriched in the geikilite component.

Comparison of Chapesvara with other complexes in the Fennoscandian Shield

In Figure 10, we compare the overall compositional trend of chromian spinel observed in the Chapesvara-I and -II complex (Figure 8) with those of the Pados-Tundra complex (Nikiforov, 2018) and other chromite-enriched intrusive bodies in the Fennoscandian Shield: the Burakovsky and Monchepluton complexes, Kola Peninsula, Russia, and the Kemi complex, Finland (Lavrov et al., 1987; Chashchin et al., 1999; Gornostayev et al., 2000; Alapieti and Huhtelin, 2005; Barkov et al., 2015). Variations in these complexes are all consistent with an Al-Cr trend at early stages and a Cr-Fe^{3+} trend at advanced and late stages. On the other hand, a distinctive characteristic of the Chapesvara-I and -II complex is the appearance of a relatively aluminous chromite at an early stage of crystallization. As a result, the Al-Cr trend is comparatively more extended and better developed in this complex (cf. Figures 8, 10).

Table 1. Compositions of silicate minerals associated with a zoned grain of chromian spinel in the Chapesvara complex.

#		SiO_2	TiO_2	Al_2O_3	Cr_2O_3	FeO_T	MnO	MgO	CaO	NiO	Na_2O	K_2O	Total
1	Ol	40.24	0.01	0.00	0.00	10.52	0.14	48.18	0.00	0.38	0.03	0.01	99.51
2		40.42	0.00	0.00	0.06	10.80	0.15	48.03	0.01	0.37	0.01	0.01	99.86
3	Chl	33.16	0.04	15.25	2.24	3.08	0.02	33.05	0.00	0.22	0.00	0.00	87.06
4		33.19	0.06	15.47	2.15	2.93	0.02	33.67	0.00	0.24	0.00	0.00	87.73
5	Opx	57.73	0.03	0.13	0.17	7.68	0.20	34.00	0.05	0.06	0.02	0.00	100.07
6	Amp	59.83	0.07	1.33	0.33	2.29	0.08	23.15	12.21	0.10	0.29	0.02	99.70
7	Opx	56.14	0.10	1.69	0.69	7.35	0.18	31.88	1.26	0.08	0.02	0.01	99.40
8	Chl	31.84	0.05	16.15	2.71	2.60	0.04	33.74	0.01	0.19	0.02	0.00	87.35
9		31.89	0.04	15.63	3.09	2.95	0.03	32.76	0.00	0.21	0.00	0.00	86.60
10		32.29	0.04	15.85	2.81	2.90	0.03	33.94	0.00	0.22	0.03	0.00	88.11
11	Ol	40.29	0.00	0.00	0.07	11.11	0.15	48.07	0.00	0.38	0.00	0.00	100.07
12		40.28	0.00	0.00	0.03	11.13	0.16	47.94	0.02	0.37	0.00	0.00	99.93
13		40.21	0.00	0.00	0.03	11.04	0.16	47.66	0.03	0.38	0.00	0.00	99.51
14	Opx	56.05	0.04	1.50	0.66	6.76	0.17	32.49	1.59	0.00	0.07	0.00	99.33
15		56.37	0.05	1.29	0.67	6.48	0.17	32.60	1.45	0.00	0.02	0.00	99.10
16		56.52	0.04	1.34	0.61	6.59	0.17	32.52	1.52	0.00	0.06	0.00	99.37
17	Amp	58.44	0.02	0.65	0.05	2.00	0.08	22.84	12.77	0.00	0.24	0.02	97.11
18		58.17	0.05	0.63	0.06	1.97	0.08	23.09	12.66	0.00	0.29	0.02	97.02

Results of WDS analyses are listed in weight %. The location of data-points number 1-10 is shown in Figure 4e. These data pertain to sample Chp-7 (Chapesvara-I body); the sampling area is shown in Figure 2a. Zero means "not detected"; FeO_T stands for total iron expressed as FeO.

Anomalous paragenesis of coexisting chromite-ilmenite at Lyavaraka

As noted, the analyzed pairs of Chr-Ilm grains form intergrowths in a pegmatitic orthopyroxene-amphibole rock (sample LVR-37A: Figure 1b), which is composed of grains of orthopyroxene up to 5 cm across associated with tremolite-actinolite and anthophyllite (Figure 11a, Table 5). The orthopyroxene grains are moderately magnesian and unzoned (Mg# 81.6-82.3; WDS). The subhedral composite chromite-ilmenite grains are enclosed in orthopyroxene (Figure 11b), thus implying that they were trapped at the time of growth in the komatiitic magma. The submicrometric lamellae of chromian magnetite ["Cr-Mgt(exs.)"] are clearly crystallographically oriented in the matrix chromite ("Chr host"; Figure 12 a,b) and likely formed by exsolution. We used the quantitative SEM/EDS approach to analyze these minute phases (Tables 6, 7). Note that areas of virtually homogeneous chromite ("Chr-hom.") exist as narrow zones in contact with platy grains of magnesian ilmenite (Ilm) located at margins of the composite oxide grains (Figures 11a, 12 a,b).

Our results of WDS and SEM/EDS analyses are in good agreement. The lamellar "Cr-Mgt(exs.)" phases could only be evaluated by the SEM/EDS (Tables 6, 7). We note that: 1) The "Chr-host" and **"**Chr-hom.**"** domains are rather similar in composition, although the latter seem to be slightly enriched in Mg-Al (the spinel component) and relatively poor in Fe^{3+}. 2) The "exsolution Cr-Mgt" phase is highly enriched in Fe^{3+} and is poor in Mg and Al. 3) The Ilm grains display the highest Mg content among all coexisting phases. The MgO content of the magnesian ilmenite (8.0-8.4 wt%) is twice that of the "exsolution Cr-Mgt" (2.8-3.3 wt%); also, it is significantly higher than that of the host and homogeneous Chr domain (≤4.5 wt% MgO: Tables 6, 7). The highly magnesian composition of the Ilm grains is shown in the Mg-distribution map (Figure 13a).

DISCUSSION

Mineralogical evidence at Lyavaraka

The Lyavaraka and Chapesvara intrusive bodies of dunite-harzburgite-orthopyroxenite in the Serpentinite Belt formed in a similar tectonic setting by inputs of essentially the same melt of komatiitic nature (cf. Barkov et al., 2019). Both Lyavaraka and Chapesvara-II display a core-like zone of Ol-Opx cumulates enriched in Mg; they display evidence of a significant buildup in the fugacity of oxygen, fO_2, during crystallization.

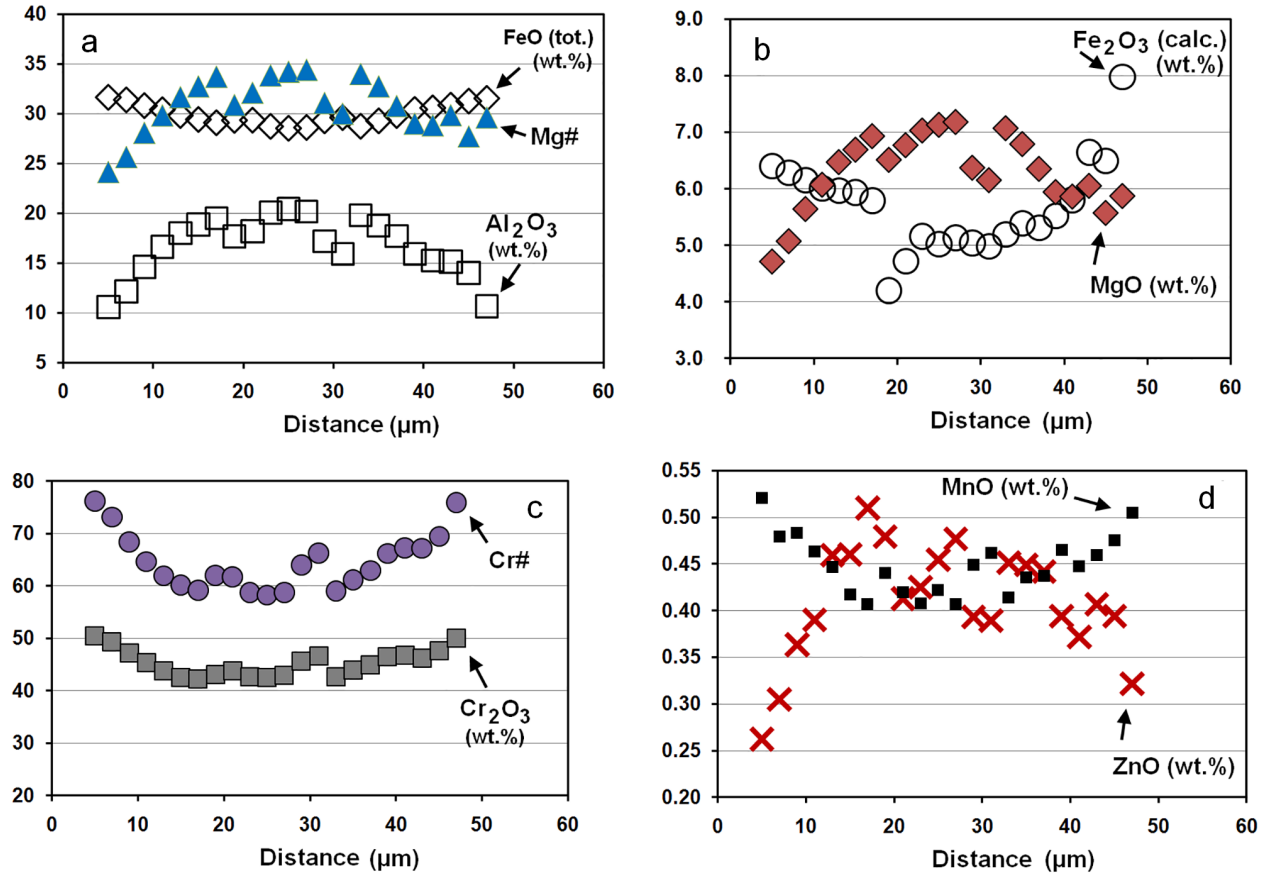

Figure 5 (a-d). Compositional variations expressed in weight% in values of total FeO, Fe_2O_3 (calculated), Al_2O_3, MgO, Cr_2O_3, minor MnO, ZnO and of the indexes Mg# [100Mg/(Mg+Fe^{2+}+Mn)] and Cr# [100Cr/(Cr+Al)] along the electron-microprobe traverse ab and across the zoned grain of chromian spinel (shown in Figure 4e).

The "homogeneous Chr phase" at Lyavaraka (Figure 12 a,b) may well reflect a primary composition of chromite before the phenomenon of exsolution occurred. Relative minima in Fe^{3+} and Fe^{3+}# in these phases (Table 7) suggest that the environment was not strongly oxidizing at this point. The "host Chr phase" crystallized nearly simultaneously. The presumed crystallization proceeded with a sharp and progressive increase in fO_2 as the temperature dropped. These conditions resulted in the development of crystallographically oriented lamellae of chromian magnetite (Figure 12 a,b). Titanium, a relatively incompatible element in this context, likely accumulated at margins of the crystallizing Chr grains, causing the deposition of rim-like zones of ilmenite (Figures 11a, 13a). The anomalous content of MgO in ilmenite, ~8 wt%, which is ~1.5 times greater than the content in the coexisting chromite (Tables 6, 7), is attributed to a sharp rise in Mg/Fe^{2+} ratio in residual portions of the Ti-enriched melt due to the pronounced conversion of Fe^{2+} to Fe^{3+} as a result of highly oxidizing conditions existing at the final stage of crystallization. A re-equilibration of chromian spinel and ilmenite at a subsolidus temperature seems unlikely, as the "homogeneous Chr phase" shows, where in contact, about the same or even slightly greater extent of magnesium enrichment as the bulk Chr phase ("host Chr").

Genetic implications at Chapesvara

The chromite present in the core of the zoned grain pertaining to the early generation (Chr-1; Figure 4e) has a Mg# value of ~35-40; it appeared on the liquidus, presumably, after crystallization of the associated olivine (Fo_{89}). Further crystallization with a normal drop in temperature led to a decrease in content of the spinel component in the magma. Consequently, contents of Mg and Al mutually decreased toward the margin of the zoned grain (Figure 4a). Experimental data are consistent, indicating that Mg is preferentially incorporated into olivine and aluminate spinel at 1300 °C (Jamieson and Roeder, 1984). The observed trends are very consistent

Table 2. Compositions of the zoned grain of chromite and associated chromian spinel of the second generation in the Chapesvara-I body.

#	μm	TiO_2	Al_2O_3	Cr_2O_3	V_2O_3	$Fe_2O_{3\,c}$	FeO_c	FeO_T	MnO	MgO	ZnO	NiO	Total
1	5	0.46	10.57	50.48	0.20	6.40	25.91	31.67	0.52	4.71	0.26	0.06	99.58
2	7	0.42	12.14	49.4	0.25	6.29	25.75	31.41	0.48	5.07	0.31	0.07	100.18
3	9	0.42	14.62	47.17	0.23	6.15	25.29	30.83	0.48	5.64	0.36	0.08	100.46
4	11	0.39	16.63	45.43	0.23	6.01	25.01	30.42	0.46	6.07	0.39	0.06	100.68
5	13	0.41	18.01	43.78	0.23	5.97	24.47	29.84	0.45	6.47	0.46	0.06	100.30
6	15	0.41	18.86	42.58	0.23	5.94	24.10	29.44	0.42	6.69	0.46	0.08	99.77
7	17	0.41	19.52	42.33	0.13	5.79	23.90	29.11	0.41	6.93	0.51	0.06	99.98
8	19	1.82	17.68	43.15	0.17	4.20	25.57	29.35	0.44	6.51	0.48	0.06	100.09
9	21	1.29	18.19	43.8	0.19	4.72	25.13	29.37	0.42	6.77	0.41	0.07	100.99
10	23	0.42	20.05	42.65	0.21	5.16	24.10	28.74	0.41	7.03	0.43	0.05	100.50
11	25	0.44	20.43	42.58	0.19	5.03	24.03	28.55	0.42	7.13	0.45	0.11	100.81
12	27	0.43	20.19	42.91	0.19	5.14	24.01	28.63	0.41	7.18	0.48	0.05	100.99
13	29	0.53	17.20	45.63	0.17	5.04	24.76	29.30	0.45	6.37	0.39	0.08	100.63
14	31	0.78	15.91	46.68	0.18	4.98	25.15	29.63	0.46	6.15	0.39	0.08	100.75
15	33	0.57	19.82	42.64	0.18	5.19	24.08	28.75	0.41	7.07	0.45	0.06	100.47
16	35	0.50	18.75	44.02	0.21	5.39	24.45	29.30	0.44	6.79	0.45	0.06	101.05
17	37	0.58	17.72	44.92	0.23	5.31	25.06	29.84	0.44	6.35	0.44	0.05	101.10
18	39	0.64	15.91	46.52	0.22	5.53	25.48	30.45	0.47	5.94	0.39	0.07	101.16
19	41	0.62	15.23	46.80	0.19	5.81	25.38	30.6	0.45	5.86	0.37	0.07	100.77
20	43	0.53	15.14	46.26	0.21	6.65	24.90	30.88	0.46	6.05	0.41	0.08	100.68
21	45	0.49	14.00	47.61	0.23	6.49	25.45	31.29	0.48	5.57	0.39	0.08	100.79
22	47	0.46	10.66	50.10	0.22	7.98	24.38	31.56	0.51	5.87	0.32	0.09	100.58
23		0.35	5.79	57.67	0.16	4.77	26.51	30.80	0.57	3.82	0.30	0.04	99.97
24		0.37	6.28	57.54	0.18	4.77	26.46	30.75	0.57	4.01	0.30	0.07	100.55
25		0.37	6.45	57.09	0.23	5.06	26.47	31.02	0.57	4.06	0.29	0.05	100.64
26		0.36	6.20	56.89	0.14	5.32	26.47	31.26	0.55	3.94	0.29	0.07	100.22
27		0.39	6.24	57.43	0.15	4.90	26.33	30.74	0.53	4.12	0.31	0.03	100.44
28		0.41	7.00	54.22	0.17	5.48	25.13	30.06	0.57	4.38	0.29	0.07	97.72
29		0.35	6.18	57.46	0.20	4.91	26.32	30.74	0.58	4.10	0.27	0.01	100.39
30		0.38	6.14	58.02	0.21	4.59	26.60	30.73	0.55	4.00	0.34	0.02	100.86

Analyses numbers 1 to 22 (traverse ab) pertain to the Chr-1 grain, and #23 to 30 pertain to the Chr-2 grain; the grains analyzed and points *a*-*b* of the traverse ab are shown in Figure 3e. FeO_T represents all Fe expressed as FeO; FeO_c and Fe_2O_{3c} are the values calculated on the basis of charge balance and a total of four atoms of oxygen per formula unit.

in the Chapesvara-I and -II bodies (Figures 6 to 8), thus implying that they belong to a single complex of subvolcanic rocks formed under similar conditions, likely from batches of essentially the same komatiitic magma. The level of the intrinsic fugacity of oxygen (fO_2) in the magma and, consequently, the content of ferric iron, clearly increased during the crystallization of the first-generation phase of Chr-1 (Figure 5b), and likely continued after the magma froze. The overall trend is consistent: the Fe^{3+}# values increased, whereas values of Mg# decreased in chromite grains with a drop in temperature accompanied by an increase in fO_2 (Figure 7). A relative buildup in ferrian chromite (so-called "ferritchromit") formed in peripheral portions (Figure 4f) and close to the margins, commonly as a diffuse rim, in chromite grains of the Chapesvara-I and -II bodies, as was previously observed

Table 3. Atomic proportions in compositions of the zoned grain of chromite and the associated chromian spinel in the Chapesvara-I body.

#	Ti	Al	Cr	V	Fe^{3+}	Fe^{2+}	Mn	Mg	Zn	Ni	Mg#	Cr#
1	0.012	0.43	1.38	0.006	0.17	0.75	0.015	0.24	0.007	0.002	24.1	76.2
2	0.011	0.49	1.33	0.007	0.16	0.73	0.014	0.26	0.008	0.002	25.6	73.2
3	0.011	0.57	1.24	0.006	0.15	0.71	0.014	0.28	0.009	0.002	28.1	68.4
4	0.010	0.64	1.18	0.006	0.15	0.69	0.013	0.30	0.009	0.002	29.8	64.7
5	0.010	0.69	1.13	0.006	0.15	0.67	0.012	0.32	0.011	0.002	31.6	62.0
6	0.010	0.73	1.10	0.006	0.15	0.66	0.012	0.33	0.011	0.002	32.7	60.2
7	0.010	0.75	1.09	0.003	0.14	0.65	0.011	0.34	0.012	0.001	33.7	59.3
8	0.045	0.68	1.12	0.005	0.10	0.70	0.012	0.32	0.012	0.002	30.9	62.1
9	0.031	0.69	1.12	0.005	0.12	0.68	0.012	0.33	0.010	0.002	32.1	61.8
10	0.010	0.76	1.09	0.005	0.13	0.65	0.011	0.34	0.010	0.001	33.8	58.8
11	0.011	0.77	1.08	0.005	0.12	0.64	0.011	0.34	0.011	0.003	34.2	58.3
12	0.010	0.76	1.09	0.005	0.12	0.64	0.011	0.34	0.011	0.001	34.4	58.8
13	0.013	0.66	1.18	0.005	0.12	0.68	0.012	0.31	0.010	0.002	31.1	64.0
14	0.019	0.62	1.22	0.005	0.12	0.69	0.013	0.30	0.009	0.002	30.0	66.3
15	0.014	0.75	1.09	0.005	0.13	0.65	0.011	0.34	0.011	0.002	34.0	59.1
16	0.012	0.71	1.12	0.006	0.13	0.66	0.012	0.33	0.011	0.001	32.7	61.2
17	0.014	0.68	1.16	0.006	0.13	0.68	0.012	0.31	0.011	0.001	30.7	63.0
18	0.016	0.62	1.21	0.006	0.14	0.70	0.013	0.29	0.010	0.002	29.0	66.2
19	0.015	0.59	1.23	0.005	0.14	0.70	0.013	0.29	0.009	0.002	28.8	67.3
20	0.013	0.59	1.21	0.006	0.17	0.69	0.013	0.30	0.010	0.002	29.8	67.2
21	0.012	0.55	1.26	0.006	0.16	0.71	0.013	0.28	0.010	0.002	27.7	69.5
22	0.012	0.43	1.34	0.006	0.20	0.69	0.014	0.30	0.008	0.002	29.6	75.9
23	0.009	0.24	1.61	0.005	0.13	0.78	0.017	0.20	0.008	0.001	20.1	87.0
24	0.010	0.26	1.59	0.005	0.13	0.77	0.017	0.21	0.008	0.002	20.9	86.0
25	0.010	0.27	1.58	0.006	0.13	0.77	0.017	0.21	0.008	0.001	21.1	85.6
26	0.009	0.26	1.58	0.004	0.14	0.78	0.016	0.21	0.007	0.002	20.6	86.0
27	0.010	0.26	1.59	0.004	0.13	0.77	0.016	0.21	0.008	0.001	21.5	86.1
28	0.011	0.29	1.53	0.005	0.15	0.75	0.017	0.23	0.008	0.002	23.3	83.9
29	0.009	0.26	1.59	0.006	0.13	0.77	0.017	0.21	0.007	0.000	21.4	86.2
30	0.010	0.25	1.60	0.006	0.12	0.78	0.016	0.21	0.009	0.001	20.8	86.4

Results of WDS analyses expressed in weight % are listed in Table 2. The Mg# index [100Mg/(Mg + Fe^{2+} + Mn)] and the Cr# index [100Cr/(Cr + Al)] are the ratios of values expressed in atoms per formula unit, apfu. The formulae and values of Fe^{2+} and Fe^{3+} were calculated on the basis of charge-balance requirements and four atoms of oxygen per formula unit.

in the Pados-Tundra complex (Barkov et al., 2017a; Nikiforov, 2018).

The relative enrichment in ferric iron, observed in late-crystallizing phases of chromite, is displayed in an example of a zoned grain (Figure 4f), which is associated with olivine ($Fo_{89.2-89.4}$) in a fine-grained dunite of the Chapesvara-II sill. The core zone (labeled "C") and peripheral areas ("P") have the following WDS compositions:TiO_2 0.49 and 0.74, Al_2O_3 17.17 and 4.55, Cr_2O_3 45.63 and 56.24,V_2O_3 0.10 and 0.22, FeO_{total} 29.13 and 33.32, $Fe_2O_{3(calc.)}$ 5.63 and 6.97, $FeO_{(calc)}$ 24.07 and 27.05, MnO 0.49 and 0.64, MgO 6.76 and 3.53, ZnO 0.50 and 0.31, NiO 0.08 and 0.10, and total 100.90 and 100.35 wt%, respectively. The formulae calculated on the basis of charge-balance requirements with a value of four atoms of oxygen per formula unit are: $(Fe^{2+}_{0.66}Mg_{0.33}Mn_{0.01}Zn_{0.01})_{\Sigma 1.01}(Cr_{1.18}Al_{0.66}Fe^{3+}_{0.14}Ti_{0.01}V_{<0.01})_{\Sigma 1.99}O_4$ and $(Fe^{2+}_{0.80}Mg_{0.19}Mn_{0.02}Zn_{0.01})_{\Sigma 1.02}$

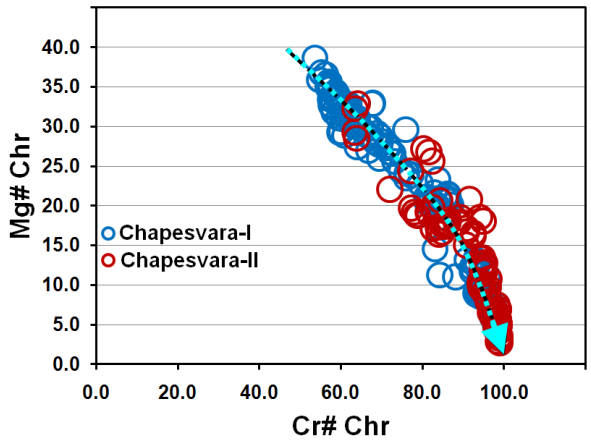

Figure 6. Plot of values of the index Mg# vs those of the Cr# index in compositions of chromite (Chr) from the Chapesvara-I and -II complex.

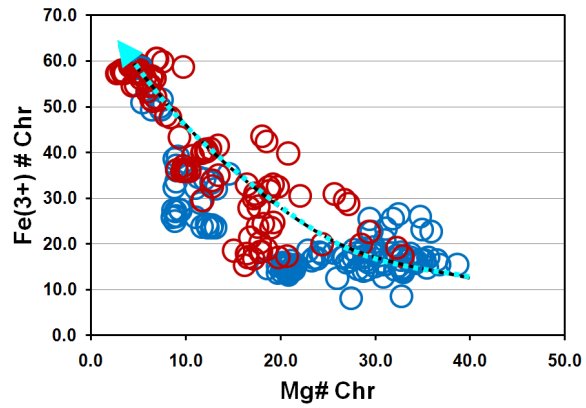

Figure 7. Plot of values of the index Mg# vs those of the index Fe^{3+}# [$100Fe^{3+}/(Fe^{3+}+Fe^{2+})$] in compositions of chromite (Chr) from the Chapesvara-I and -II complex.

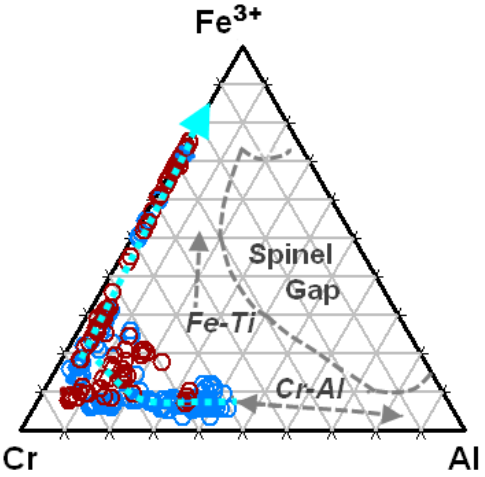

Figure 8. Compositions of chromian spinel from the Chapesvara-I and -II complex in the Cr-Fe^{3+}-Al compositional space. The Fe-Ti and Cr-Al trends and the spinel gap area are after Barnes, Roeder (2001).

$(Cr_{1.58}Al_{0.19}Fe^{3+}_{0.19}Ti_{0.02}V_{<0.01})_{\Sigma 1.98}O_4$.

The early-nucleated core and the peripheral zones that crystallized at a late stage in a H_2O-saturated medium, as implied by the presence of clinochlore inclusions, recall the sequential development of the two generations of chromite grains (cf. Figure 4c). The inferred buildup in Fe^{3+} can be more pronounced, e.g., in rim-like or peripheral zones having Fe^{3+}#=44 (*vs* 29 in the central areas) in grains of disseminated chromite in the Upper contact facies of the Chapesvara-II sill (cf. Barkov et al., 2019).

The second generation of chromite, represented by the Chr-2 grains (Figure 4 c,e) began to nucleate shortly after grains of the Chr-1 generation formed. The later generation was deposited at a stage when levels of H_2O had increased dramatically in the remaining portions of the late melt. As a result, numerous inclusions of clinochlore formed from trapped portions of H_2O-enriched fluid, presumably at a temperature ≤880 ºC, which represents the upper limit of thermal stability of clinochlore (cf., Chernosky, 1974; Staudigel and Schreyer, 1977). Correspondingly, the clinochlore lamellae crystallized syngenetically along the crystallographically defined growth directions in the host phase (Figure 4c). The observations reported at Pados-Tundra are relevant: more than 80% of grains of laurite [$Ru(S,Se)_2$] occur as two-phase inclusions laurite +clinochlore hosted by magnesiochromite-chromite; they crystallized from microvolumes of H_2O-bearing fluid enriched in Ru, S, and lithophile elements (Barkov et al., 2017b).

We report an unusual pattern of decoupling of Zn from Mn during the formation of primary zoning in chromite. These elements are expected to behave uniformly (e.g., Barnes, 2000, and references therein). However, in our case, Zn increases toward the core, whereas Mn displays the opposite trend, increasing toward the margin (Figure 5d). The host rock is fairly fresh and unaffected by regional metamorphism; these patterns of zonation thus are primary. The same behavior of Zn and Mn is implied in zoned grains of chromite-magnesiochromite in chromitites of the Pados-Tundra complex (Barkov et al., 2017b). The latter authors reported the following mean values (and ranges) in the core of magnesiochromite phase: MgO 10.37 (9.17-11.71), MnO 0.99 (0.80-1.11), and ZnO 0.82 (0.64-1.04), with a mean Mg# ~50. The rim phase contains: MgO 6.79 (5.29-8.36), MnO 1.32 (0.91-1.51), and ZnO 0.45 (0.23-0.59); Mg#=~35. The

Table 4. Representative results of electron-microprobe analyses of coexisting chromian spinel and ilmenite in the Chapesvara-I and Chapesvara-II bodies.

#			TiO_2	Al_2O_3	Cr_2O_3	V_2O_3	FeO_T	MnO	MgO	ZnO	NiO	Total	Mg#
1	CHP-2	Chr	2.12	1.96	51.59	0.30	41.00	0.44	1.69	0.56	0.13	100.92	8.8
2		Chr	0.98	2.32	52.50	0.35	41.14	0.47	1.77	0.53	0.03	101.35	9.4
3		Ilm	53.80	0.00	0.17	0.55	41.90	0.52	3.61	0.01	0.02	100.57	13.2
4		Ilm	53.39	0.01	0.78	0.59	41.35	0.55	3.50	0.03	0.07	100.27	13.0
5		Ilm	50.21	0.11	3.71	0.52	40.68	0.48	4.02	0.03	0.04	99.80	14.8
6	CHP-3	Chr	2.41	5.20	41.43	0.42	47.39	0.46	2.24	0.44	0.20	102.02	11.3
7		Chr	5.83	1.85	46.81	0.33	41.08	0.50	2.08	0.54	0.10	100.0	9.9
8		Ilm	52.51	0.00	2.36	0.63	41.22	0.50	4.03	0.01	0.06	101.32	14.7
9		Ilm	52.27	0.00	2.72	0.63	41.30	0.54	3.96	0.02	0.10	101.54	14.4
10	CHP-5	Chr	1.62	0.25	17.82	0.28	75.04	0.29	0.89	0.09	0.55	101.72	4.8
11		Chr	1.67	0.24	17.42	0.19	74.70	0.29	0.93	0.12	0.53	100.96	5.1
12		Ilm	52.55	0.00	0.25	0.57	42.15	0.72	3.51	0.00	0.11	99.86	12.7
13		Ilm	52.97	0.00	0.24	0.63	42.03	0.70	3.65	0.01	0.09	100.32	13.2
14	CHP-11	Chr	0.89	2.62	54.41	0.19	37.60	0.58	2.40	0.32	0.10	100.13	12.8
15		Chr	0.87	2.77	54.88	0.23	37.48	0.56	2.48	0.35	0.08	100.67	13.2
16		Ilm	53.45	0.00	2.22	0.58	39.35	0.67	5.03	0.00	0.13	101.42	18.3
17		Ilm	52.93	0.00	2.01	0.63	40.89	0.69	4.18	0.05	0.07	101.45	15.2
18		Ilm	54.05	0.00	1.58	0.65	38.35	0.59	5.75	0.04	0.16	101.16	20.8
19	CHP-13	Chr	1.24	1.90	51.40	0.39	40.92	0.58	2.17	0.40	0.09	100.41	11.5
20		Chr	1.37	5.82	42.56	0.49	44.53	0.54	2.80	0.40	0.12	100.37	14.5
21		Ilm	50.65	0.00	1.83	0.64	40.26	0.65	5.25	0.04	0.06	99.37	18.6
22		Ilm	50.17	0.00	2.20	0.60	39.77	0.63	5.80	0.04	0.08	99.29	20.4
23	CHP-18	Chr	1.63	0.17	17.12	0.28	75.98	0.37	0.87	0.11	0.43	101.94	4.7
24		Chr	1.52	0.19	17.11	0.24	74.91	0.47	1.40	0.16	0.35	101.32	7.5
25		Ilm	53.23	0.00	0.22	0.53	41.35	1.11	3.92	0.04	0.04	100.44	14.1
26		Ilm	53.28	0.00	0.24	0.58	41.46	1.02	3.69	0.01	0.11	100.39	13.4
27	CHP-19	Chr	1.80	0.18	19.72	0.22	73.40	0.43	0.95	0.14	0.44	101.97	5.1
28		Ilm	53.20	0.00	0.20	0.63	41.30	1.04	3.95	0.01	0.06	100.39	14.3
29		Ilm	52.84	0.00	0.19	0.61	41.77	1.13	3.52	0.02	0.11	100.20	12.8
30	CHP-19A	Chr	1.66	0.21	20.47	0.21	71.83	0.45	0.93	0.15	0.42	100.89	5.0
31		Chr	1.65	0.16	19.96	0.23	72.19	0.46	0.92	0.13	0.41	100.72	5.0
32		Ilm	52.38	0.00	0.23	0.55	42.53	1.25	2.78	0.01	0.02	99.75	10.2
33		Ilm	52.26	0.00	0.19	0.59	41.60	1.16	3.39	0.03	0.05	99.28	12.4
34	CHP-21	Chr	1.06	1.82	45.38	0.29	44.82	0.54	1.89	0.37	0.09	98.07	10.4
35		Chr	0.91	1.95	45.87	0.30	44.58	0.55	1.89	0.32	0.10	98.26	10.4
36		Ilm	51.17	0.00	0.42	0.67	43.50	0.65	2.96	0.00	0.07	99.44	10.7
37		Ilm	51.57	0.00	0.25	0.65	43.11	0.60	3.38	0.01	0.06	99.63	12.1

Results of WDS analyses are listed in weight %. Chr is chromian spinel; Ilm is ilmenite. Samples CHP-1 to 13 pertain to the Chapesvara-I body, CHP-16 to 21 pertain to the Chapesvara-II body (Figure 2 a,b). Mg#=100Mg/(Mg+Fe^{2+}+Mn). The majority of the ilmenite grains analyzed form inclusions hosted by Chr grains, except for numbers #3, 4, 25, 26, 28, 29, 32 and 33, which represent separated grains associated with Chr. Zero means "not detected". FeO_T stands for total iron expressed as FeO.

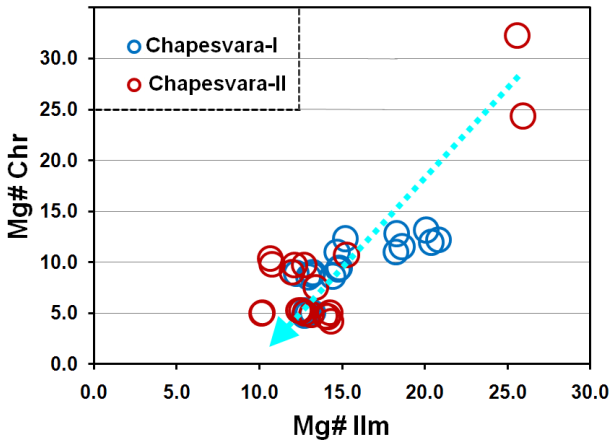

Figure 9. Plot of values of the index Mg# in compositions of coexisting phases of chromite (Chr) and ilmenite (Ilm) in the Chapesvara-I and -II complex.

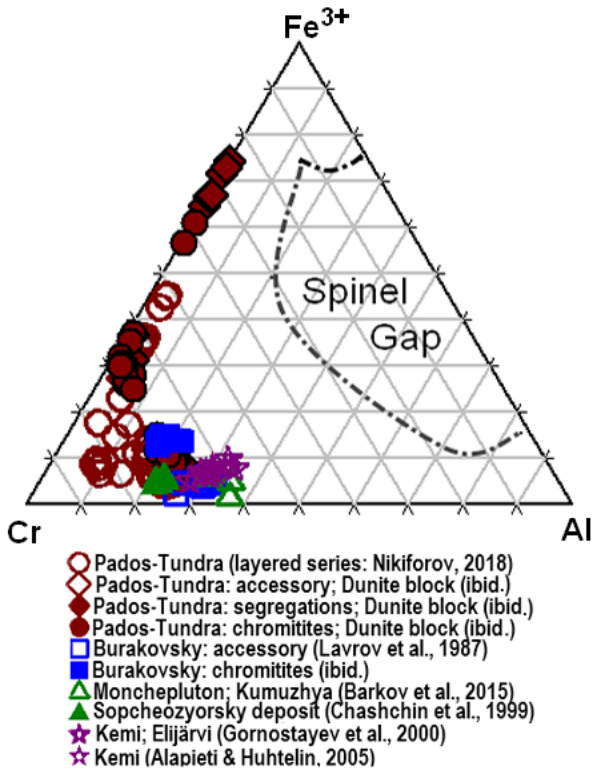

Figure 10. Compositions of chromian spinel from chromitites and chromite-bearing lithologies in Paleoproterozoic ultramafic-mafic complexes of the Fennoscandian Shield: Pados-Tundra (Nikiforov, 2018), Burakovsky (Lavrov et al., 1987), Monchepluton (Chashchin et al., 1999; Barkov et al., 2015), Russia and Kemi, Finland (Gornostayev et al., 2000; Alapieti and Huhtelin, 2005) in the Cr-Fe^{3+}-Al compositional space.

core is thus notably more magnesian and enriched in Zn, though the composition remains fairly magnesian at the margin. Therefore, Zn clearly joins Mg in patterns of early fractionation in chromite grains at both Chapesvara and Pados-Tundra.

We document the progressive development of an anomalous character of Fe-Mg partitioning between chromite and ilmenite. Similar to the paragenesis at Lyavaraka, the ilmenite phase is invariably richer in Mg than the associated chromite (Table 4, Figure 9). The possible presence of minor amounts of Fe^{3+}_{calc} (0.04-0.1 *apfu*) requires an analytical confirmation in ilmenite. The ratio of Mg# in ilmenite to Mg# in chromite attains 2-2.5 in coexisting phases. Note, however, that this ratio is close to 1:1 in the case of most Mg-enriched compositions of chromite (Figure 9). Such tendency implies that the Fe-Mg distribution was closer to being normal at the early stage of the Chr-Ilm paragenesis. We thus believe that this anomaly reflects the progressive increase in the level of oxidation in the remaining portions of the magma as it neared the solidus and even after crystallization of the melt was complete. The pattern of oxidation led to the enhanced conversion of Fe^{2+} to Fe^{3+}, causing an anomalous buildup in the ratio Mg/Fe^{2+} in residual droplets of the melt from which the magnesian ilmenite formed. The general process of progressive oxidation at Chapesvara-I and -II could well be related to the gradual loss of hydrogen by diffusion through the magma during its crystallization (Czamanske and Wones, 1973), which would cause the magma to become intrinsically oxygenated in a progressive way.

CONCLUSIONS

1) The observed variations and compositional trends of chromite in the Chapesvara-I and Chapesvara-II bodies are very similar. These bodies belong to a single subvolcanic intrusive complex of dunite - harzburgite - orthopyroxenite suites that crystallized from a komatiitic magma (cf. Barkov et al., 2019). There are notable similarities of some characteristics of the Cr-Ti mineralization with that of the Pados-Tundra igneous complex, which forms part of the same trend in the Serpentinite Belt in the Kola Peninsula. The Lyavaraka dunite-harzburgite-orthopyroxenite complex was emplaced in essentially the same tectonic setting, belongs to the latter Belt, and displays striking similarities in the anomalous character of chromite - ilmenite mineralization.

2) Two generations of chromian spinel exist in the Chapesvara complex. Grains of the first generation are relatively enriched in Mg and are essentially free of inclusions. The second generation is poorer in Mg and is full of inclusions of clinochlore that crystallized from trapped portions of aqueous fluid. These occurrences

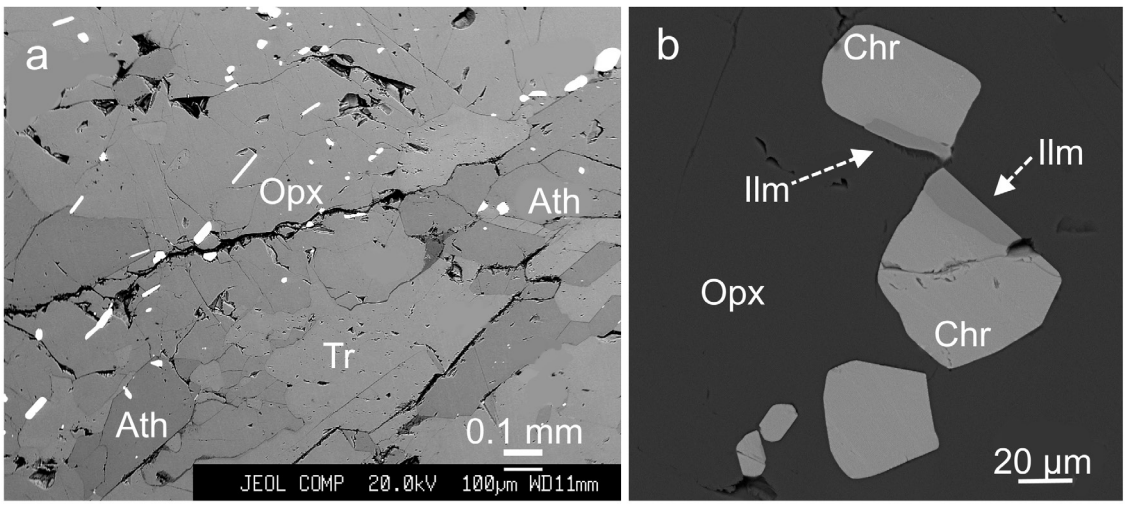

Figure 11 (a, b). Back-scattered electron images showing the pegmatitic orthopyroxene (Opx) - amphibole rock (Figure 11a) consisting of tremolite (Tr) and anthophyllite (Ath) from the Lyavaraka complex. Figure 11b shows accessory grains of chromite (Chr) and ilmenite (Ilm) hosted by orthopyroxene (Opx) in this rock (sample LVR-37A).

Table 5. Compositions of orthopyroxene and amphiboles associated with Chr – Ilm intergrowths in the Lyavaraka complex.

#		SiO_2	TiO_2	Al_2O_3	Cr_2O_3	FeO_T	MnO	MgO	CaO	Na_2O	K_2O	Total	Mg#
1	Opx	55.64	0.03	2.96	0.44	9.35	0.20	30.53	0.11	0.00	0.00	99.26	81.9
2		55.77	0.05	2.87	0.38	9.28	0.23	30.47	0.11	0.00	0.00	99.16	81.6
3		56.41	0.04	2.22	0.14	9.29	0.22	30.86	0.12	0.00	0.00	99.30	81.7
4		56.32	0.04	2.18	0.13	9.26	0.23	31.01	0.13	0.00	0.00	99.30	82.3
5		56.67	0.03	1.95	0.09	9.16	0.23	30.95	0.12	0.00	0.00	99.20	81.6
6		56.66	0.03	1.89	0.10	9.15	0.22	30.97	0.12	0.00	0.00	99.14	81.6
7	Tr	52.93	0.26	6.34	0.61	3.80	0.08	19.42	12.34	0.75	0.09	96.62	90.0
8		52.75	0.28	6.22	0.62	3.78	0.09	19.48	12.35	0.70	0.09	96.36	90.1
9		52.97	0.28	6.43	0.53	4.05	0.09	19.16	12.35	0.78	0.09	96.73	89.3
10		53.09	0.29	6.38	0.57	4.06	0.09	19.27	12.28	0.80	0.10	96.93	89.3
11	Ath	58.66	0.05	1.83	0.21	8.43	0.26	27.14	0.61	0.09	0.01	97.29	84.7
12		58.46	0.04	1.90	0.22	8.46	0.26	27.13	0.59	0.10	0.00	97.16	84.7
13		58.14	0.03	2.30	0.31	8.50	0.27	27.17	0.52	0.16	0.00	97.40	84.6
14		58.40	0.05	2.32	0.28	8.46	0.24	27.47	0.54	0.22	0.00	97.98	84.8

Results of WDS analyses done on the pegmatitic Opx-Amp rock (Figure 11a) analyzed in sample LVR-37A collected in the Lyavaraka complex (Figure 1b). Opx is orthopyroxene, Tr is tremolite-actinolite, and Ath is anthophyllite. Zero means not detected. FeO_T stands for total iron expressed as FeO.

of clinochlore resemble those in the laurite-clinochlore intergrowths hosted by grains of magnesiochromite-chromite at Pados-Tundra (Barkov et al., 2017b).

3) We report on an unusual decoupling pattern of behavior of minor Zn and Mn during the crystallization of chromite. Zinc is preferably incorporated into the core with Mg. In contrast, Mn displays the expected distribution and a relative enrichment at the margin. A related behavior is displayed by these elements in compositions of zoned grain of magnesiochromite-chromite in the Pados-Tundra layered complex. These features thus appear to be characteristic of chromian spinel in the Serpentinite Belt.

4) The development of lamellae of chromiferous magnetite in the chromite matrix at Lyavaraka is highly unusual. This phenomenon may well shed light on the mechanism of transformation of chromite into magnetite

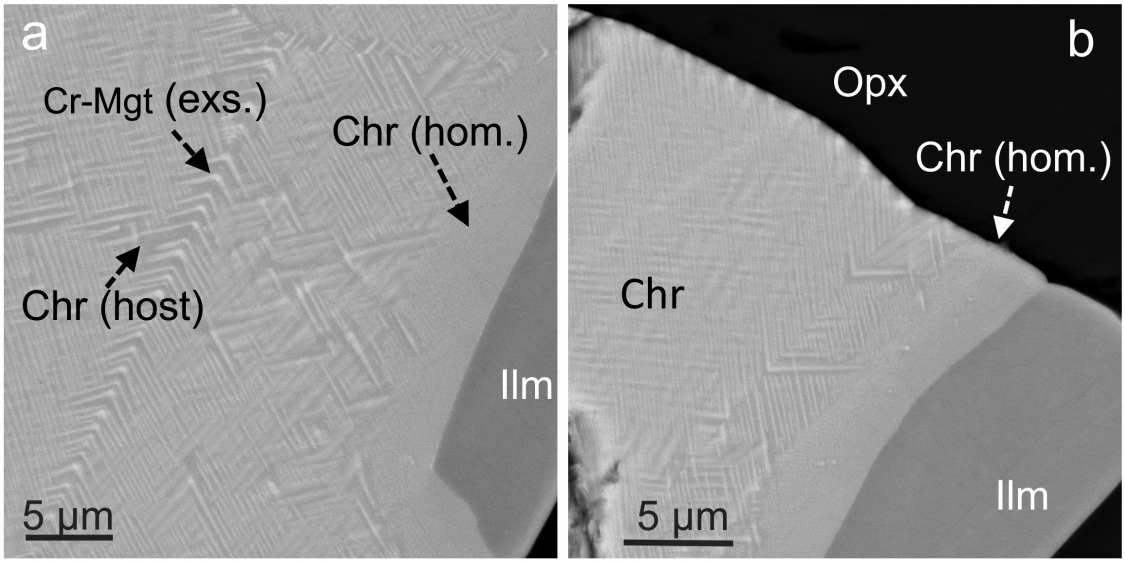

Figure 12 (a, b). Scanning-electron images of the chromite - ilmenite grains from Lyavaraka, which are present in Figure 11b. Label "Chr (hom.)" pertains to the homogeneous area of chromite, and "Chr-host", to the matrix phase of chromite that hosts lamellae of chromian magnetite, formed via exsolution, oriented crystallographically and labeled "Cr-Mgt (exs.)". The label Ilm represents magnesian ilmenite. The host is orthopyroxene, Opx [$Wo_{0.2\text{-}0.3}En_{85.4}Fs_{14.4}$] (Figure 12b).

following a sudden increase in fO_2 at an advanced stage of crystallization.

5) In the Chapesvara and Lyavaraka complexes of the Serpentinite Belt, we document new mineralogical implications of a progressive buildup in levels of fO_2, judged to be responsible for the anomalous enrichment of magnesium in magnesian ilmenite relative to the coexisting chromian spinel. The same petrogenetic mechanism of hydrogen loss leading to elevated levels of O_2 was previously inferred to operate in zoned grains of chromite (Barkov et al., 2009) and pyroxene (Barkov and Martin, 2015). Also, related effects of elevated values of fO_2 are considered to have caused hypermagnesian compositions of olivine in chromite-enriched lithologies hosted by layered intrusions in the Kola Peninsula (Barkov et al., 2020).

ACKNOWLEDGEMENTS

We thank the anonymous referees and members of the editorial board for constructive comments and useful suggestions. A.Y.B. gratefully acknowledges a partial support of this investigation by the Russian Foundation for Basic Research (project # RFBR 19-05-00181). Support from the Cherepovets State University is appreciated. V.N.K. acknowledges that the present work was also done on the state assignment of IGM SB RAS, supported by the Ministry of Science and Higher Education of the Russian Federation. Permission to access and reproduce of materials from unpublished reports was granted by the Department of Mineral Resources of Northwestern Federal District (Sevzapnedra) of the Federal Agency for Mineral Resources of the Russian Federation.

We remember warmly the late Sergey S. Kramzaev (ChSU, Cherepovets), and acknowledge his efforts and invaluable assistance during field investigations of the Chapesvara and Lyavaraka complexes.

REFERENCES

Alapieti T.T. and Huhtelin T.A., 2005. The Kemi intrusion and associated chromitite deposit. In: Early Palaeoproterozoic (2.5-2.4) Tornio-Näränkävaara layered intrusion belt and related chrome and platinum-group element mineralization, northern Finland (T.T. Alapieti, A.J. Kärki, Eds.). Field trip guidebook for the 10-th Platinum Symposium, Oulu, Finland, 2005. Geological Survey of Finland, Guide 51a, 13-32.

Balagansky V.V., Gorbunov I.A., Mudruk S.V., 2016. Palaeoproterozoic Lapland-Kola and Svecofennian Orogens (Baltic Shield). Herald (Vestnik) of the Kola Science Centre of the RAS, 3(26), 5-11 (in Russian).

Barkov A.Y., Nixon G.T., Levson V.M., Martin R.F., 2009. Patterns of zonation in magnesiochromite-chromite from placers of British Columbia, Canada. The Canadian Mineralogist 47, 953-968.

Barkov A.Y. and Martin R.F., 2015. Anomalous Cr-rich zones in sector-zoned clinopyroxene macrocrysts in gabbro, Mont Royal, Montreal, Quebec, Canada. The Canadian Mineralogist 53. 895-910.

Barkov A.Y., Nikiforov A.A., Martin, R.F., 2015. A novel mechanism of spheroidal weathering: a case study from the

Table 6. Compositions of coexisting chromite and ilmenite hosted by orthopyroxene in the Lyavaraka complex.

	#	TiO_2	Al_2O_3	Cr_2O_3	V_2O_3	$Fe_2O_{3\,c}$	FeO_c	FeO_T	MnO	MgO	ZnO	NiO	Total
Chr host	1	1.00	6.99	30.92	0.49	29.35	27.69	54.10	0.34	3.57	n.a.	0.40	100.75
Chr host	2	1.10	7.16	30.93	0.42	29.14	27.61	53.83	0.42	3.66	n.a.	0.42	100.87
Chr host	3	1.45	8.37	32.82	0.37	25.17	27.39	50.04	0.36	3.97	0.39	0.35	100.66
Chr host	4	0.87	7.35	31.89	0.40	28.35	27.23	52.74	0.48	3.77	n.a.	0.33	100.68
Chr host	5	0.89	7.20	32.13	0.45	28.57	27.54	53.25	0.42	3.69	n.a.	0.38	101.28
Chr host	6	1.00	7.43	32.04	0.42	27.98	27.68	52.86	0.34	3.70	n.a.	0.36	100.97
Chr host	7	0.99	7.85	33.34	0.37	25.41	26.89	49.75	0.47	3.89	n.a.	0.38	99.60
Chr host	8	1.05	7.89	33.07	0.45	25.47	26.85	49.77	0.47	3.99	n.a.	0.33	99.60
Chr host	9	1.55	8.31	31.11	0.40	26.16	27.16	50.70	0.33	4.14	n.a.	0.44	99.60
Chr host	10	1.53	8.62	33.15	0.40	23.68	27.13	48.44	0.48	4.17	n.a.	0.31	99.48
Chr host	11	1.13	7.15	30.76	0.39	28.28	28.16	53.61	0.00	3.58	n.a.	0.00	99.45
Chr host	12	0.85	7.02	29.74	0.47	30.85	27.24	55.00	0.45	3.64	0.30	0.19	100.74
Chr host	13	0.84	7.17	29.58	0.38	30.81	27.05	54.77	0.44	3.74	0.28	0.18	100.47
Chr host	14	0.96	7.16	30.23	0.33	30.66	27.52	55.11	0.44	3.72	0.27	0.18	101.46
Chr host	15	0.92	7.18	30.39	0.43	30.52	27.55	55.02	0.41	3.74	0.20	0.22	101.57
Chr hom.	16	1.48	8.49	34.88	0.42	22.56	27.55	47.85	0.44	4.05	n.a.	0.28	100.15
Chr hom.	17	1.56	9.65	35.78	0.39	20.64	26.79	45.36	0.43	4.52	0.30	0.45	100.51
Chr hom.	18	1.95	9.29	34.47	0.43	21.21	27.60	46.69	0.32	4.25	0.39	0.28	100.19
Cr Mgt exs.	19	0.84	5.66	25.61	0.33	35.49	27.79	59.72	0.40	2.78	n.a.	0.59	99.49
Cr Mgt exs.	20	0.92	6.33	27.67	0.42	33.48	27.75	57.88	0.36	3.33	n.a.	0.41	100.68
Ilm	21	54.81	0.15	0.69	0.00	-	-	36.01	0.62	8.22	n.a.	0.24	100.73
Ilm	22	54.91	0.26	0.78	0.00	-	-	35.74	0.65	8.07	n.a.	0.29	100.69
Ilm	23	54.89	0.15	1.09	0.00	-	-	35.41	0.71	8.24	n.a.	0.00	100.48
Ilm	24	55.52	0.15	0.97	0.00	-	-	35.29	0.73	8.34	n.a.	0.20	101.19
Ilm	25	55.08	0.15	1.21	0.00	-	-	35.82	0.73	8.30	n.a.	0.25	101.54
Ilm	26	55.15	0.00	0.81	0.00	-	-	35.93	0.66	8.01	n.a.	0.00	100.56
Ilm	27	54.08	0.00	0.64	0.07	-	-	36.07	0.68	7.97	0.01	0.06	99.58
Ilm	28	54.03	0.00	0.67	0.05	-	-	35.9	0.66	7.96	0.06	0.07	99.41
Ilm	29	52.96	0.00	0.63	0.00	-	-	37.07	0.65	8.26	0.04	0.10	99.71
Ilm	30	52.96	0.02	0.66	0.00	-	-	37.16	0.67	8.38	0	0.07	99.91

These results of microprobe analyses were obtained on grains shown in Figures 11b and 12a, b (sample LVR-37A: the location is shown in Fig. 1b). The notation "Chr host" refers to the matrix phase of chromite, whereas "Chr hom." refers to homogeneous portions of the chromite grains. The notation "Cr Mgt exs." refers to lamellae of chromian magnetite formed *via* exsolution. The symbol Ilm refers to the coexisting ilmenite (Figs. 12a, b). These intergrowths are hosted by orthopyroxene: $Wo_{0.2–0.3}En_{85.4}Fs_{14.4}$. Zero means not detected; n.a. is not analyzed. Analyses number 12–15 and 27–30 pertain to results of WDS analyses done using a JEOL JXA-8100 microprobe. The rest of the data-points listed are results of quantitative SEM/EDS analyses done using a MIRA 3 LMU system (Tescan Ltd.) combined with INCA Energy 450+ XMax 80 (Oxford Instruments Ltd.) facilities. FeO_T stands for total iron expressed as FeO, whereas FeO_c and $Fe_2O_{3\,c}$ are the values calculated on the basis of charge-balance requirements.

Monchepluton layered complex, Kola Peninsula, Russia. Bulletin of the Geological Society of Finland 87, 79-85.

Barkov A.Y., Nikiforov A.A., Halkoaho T.A.A., Konnunaho J.P., 2016. The origin of spheroidal patterns of weathering in the Pados-Tundra mafic-ultramafic complex, Kola Peninsula, Russia. Bulletin of the Geological Society of Finland 88, 105-113.

Barkov A.Y., Nikiforov A.A., Martin R.F., 2017a. The structure and cryptic layering of the Pados-Tundra ultramafic complex, Serpentinite belt, Kola Peninsula, Russia. Bulletin of the

Table 7. Atom proportions in coexisting chromite and ilmenite hosted by orthopyroxene in the Lyavaraka complex.

#	Ti	Al	Cr	V	Fe^{3+}	Fe^{2+}	Mn	Mg	Zn	Ni	Mg#	Cr#	Fe^{3+}#
1	0.027	0.29	0.86	0.014	0.78	0.82	0.010	0.19	0.000	0.011	18.5	74.8	48.8
2	0.029	0.30	0.86	0.012	0.77	0.81	0.013	0.19	0.000	0.012	18.9	74.3	48.7
3	0.038	0.34	0.91	0.010	0.66	0.80	0.011	0.21	0.010	0.010	20.3	72.4	45.3
4	0.023	0.30	0.89	0.011	0.75	0.80	0.014	0.20	0.000	0.009	19.5	74.4	48.4
5	0.023	0.30	0.89	0.013	0.75	0.81	0.013	0.19	0.00	0.011	19.1	75.0	48.3
6	0.027	0.31	0.89	0.012	0.74	0.81	0.010	0.19	0.000	0.010	19.1	74.3	47.6
7	0.026	0.33	0.93	0.011	0.68	0.80	0.014	0.21	0.000	0.011	20.2	74.0	46.0
8	0.028	0.33	0.92	0.013	0.68	0.79	0.014	0.21	0.000	0.010	20.7	73.8	46.0
9	0.041	0.35	0.87	0.011	0.69	0.80	0.010	0.22	0.000	0.013	21.2	71.5	46.4
10	0.040	0.36	0.92	0.011	0.63	0.80	0.014	0.22	0.000	0.009	21.2	72.1	44.0
11	0.030	0.30	0.87	0.011	0.76	0.84	0.00	0.19	0.000	0.00	18.5	74.3	47.5
12	0.023	0.29	0.83	0.013	0.82	0.80	0.014	0.19	0.008	0.005	19.0	74.0	50.5
13	0.022	0.30	0.83	0.011	0.82	0.80	0.013	0.20	0.007	0.005	19.5	73.5	50.6
14	0.025	0.30	0.84	0.009	0.81	0.81	0.013	0.19	0.007	0.005	19.2	73.9	50.1
15	0.024	0.30	0.84	0.012	0.80	0.81	0.012	0.19	0.005	0.006	19.2	74.0	49.9
16	0.039	0.35	0.97	0.012	0.59	0.81	0.013	0.21	0.000	0.008	20.5	73.4	42.4
17	0.040	0.39	0.98	0.011	0.54	0.77	0.013	0.23	0.008	0.013	22.8	71.3	40.9
18	0.051	0.38	0.95	0.012	0.56	0.80	0.009	0.22	0.010	0.008	21.3	71.3	40.9
19	0.023	0.24	0.73	0.010	0.97	0.84	0.012	0.15	0.000	0.017	14.9	75.2	53.5
20	0.025	0.27	0.78	0.012	0.90	0.83	0.011	0.18	0.000	0.012	17.4	74.6	52.1
21	0.98	0.004	0.013	0.000	-	0.71	0.01	0.29	0.000	0.005	28.6	-	-
22	0.98	0.007	0.015	0.000	-	0.71	0.01	0.28	0.000	0.005	28.3	-	-
23	0.98	0.004	0.020	0.000	-	0.70	0.01	0.29	0.000	0.000	28.9	-	-
24	0.98	0.004	0.018	0.000	-	0.69	0.01	0.29	0.000	0.004	29.2	-	-
25	0.97	0.004	0.023	0.000	-	0.70	0.01	0.29	0.000	0.005	28.8	-	-
26	0.98	0.000	0.015	0.000	-	0.71	0.01	0.28	0.000	0.000	28.1	-	-
27	0.98	0.000	0.012	0.001	-	0.72	0.01	0.29	0.003	0.001	27.9	-	-
28	0.98	0.000	0.013	0.001	-	0.72	0.01	0.29	0.014	0.001	28.0	-	-
29	0.96	0.000	0.012	0.000	-	0.75	0.01	0.30	0.010	0.002	28.1	-	-
30	0.96	0.001	0.013	0.000	-	0.75	0.01	0.30	0.000	0.001	28.3	-	-

Results of these analyses expressed in weight % are listed in Table 6. The Mg# index is defined as [100Mg/(Mg + Fe^{2+} + Mn); the Cr# index is [100Cr/(Cr + Al)], and the Fe^{3+}# index is [100 Fe^{3+}/(Fe^{3+} + Fe^{2+})]. Values of Fe^{2+} and Fe^{3+} were calculated on the basis of charge-balance requirements.

Geological Society of Finland 89, 35-56.

Barkov A.Y., Nikiforov A.A., Tolstykh N.D., Shvedov G.I., Korolyuk V.N., 2017b. Compounds of Ru-Se-S, alloys of Os-Ir, framboidal Ru nanophases and laurite-clinochlore intergrowths in the Pados-Tundra complex, Kola Peninsula, Russia. European Journal of Mineralogy 29, 613-622.

Barkov A.Y., Korolyuk V.N., Barkova L.P., Martin R.F., 2019. Double-front crystallization in the Chapesvara ultramafic subvolcanic complex, Serpentinite Belt, Kola Peninsula, Russia. Minerals 10, 14.

Barkov A.Y., Martin R.F., Izokh A.E., Nikiforov A.A., Korolyuk V.N., 2020. Hypermagnesian olivine in the layered complexes Monchepluton (Fo_{96}) and Pados-Tundra (Fo_{93}), Kola Peninsula. Russian Geology and Geophysics (in press, doi: 10.15372/GiG2020112).

Barnes S.J., 2000. Chromite in komatiites. II. Modification during greenschist to mid-amphibolite facies metamorphism. Journal of Petrology 41, 387-409.

Barnes S.J. and Roeder, P., 2001. The range of spinel compositions in terrestrial mafic and ultramafic rocks. Journal

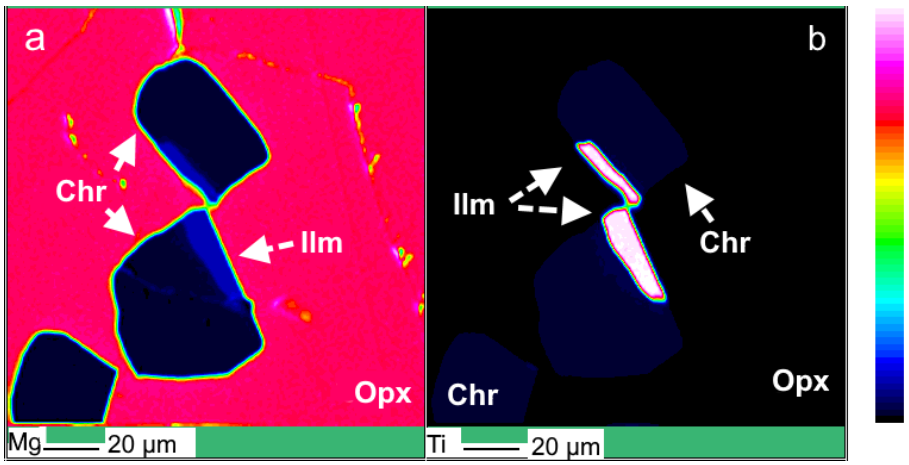

Figure 13 (a, b). Element-distribution maps show variations in contents of Mg (Figure 13a) and Ti (Figure 13b) in the coexisting chromite-ilmenite grains from Lyavaraka, which are present in Figure 11b. The attached scale represents the order of changes of relative concentrations from low (bottom) to high levels (top). The symbols used are the same as those in Figure 11b.

of Petrology 42, 2279-2302.

Chashchin V.V., Galkin A.S., Ozeryanskii V.V., Dedyukhin A.H., 1999. Sopcheozyorsky deposit of chromite and its platinum potential, Monchegorsky pluton (Kola Peninsula, Russia). Geology of Ore Deposits 41, 507-515 [in Russian].

Chernosky J.V. Jr., 1974. The upper stability of clinochlore at low pressure and the free energy of formation Mg-cordierite. The American Mineralogist 59, 496-507.

Czamanske G.K. and Wones D.R., 1973. Oxidation during magmatic differentiation, Finnmarka complex, Oslo area, Norway. 2. Mafic silicates. Journal of Petrology 14, 349-380.

Dokuchaeva V.S., 1981. The geology and ore potential of the Mount Lyavaraka massif. In Geology of Ore Deposits in the Kola Peninsula. Kola Science Centre, Apatity, 34-45 [in Russian].

Gornostayev S.S., Laajoki K.V.O., Leinonen O., 2000. New data on mineralogy of main chromitite layer of the Kemi deposit, Finland. In: Reviewed abstracts volume, GeoCanada 2000: the millennium geoscience summit, extended abstract 88, Calgary, Canada, May 2000.

Jamieson H.E. and Roeder P.L., 1984. The distribution of Mg and Fe^{2+} between olivine and spinel at 1300 °C. American Mineralogist 69, 283-291.

Korolyuk V.N., Usova L.V., Nigmatulina E.N., 2009. On the accuracy of determining composition of principal rock-forming silicates and oxides with a Jeol JXA-8100 electron microprobe. Journal of Analytical Chemistry 64, 1042-1046.

Lavrent'ev Yu.G., Korolyuk V.N., Usova L.V., Nigmatulina E.N., 2015. Electron probe microanalysis of rock-forming minerals with a Jeol JXA-8100 electron probe microanalyzer. Russian Geology and Geophysics 56, 1428-1436.

Lavrov M.M., Rezhenova S.A., Trofimov N.N., 1987. The composition of chromian spinels of the Burakovsky layered intrusion. In: Proceedings on the metallogeny of Karelia. Institute of Geology of the Karelian Science Centre of the RAS, Petrozavodsk, 138-151 [in Russian].

Mamontov V.P. and Dokuchaeva V.S., 2005. The geology and ore potential of the Pados-Tundra massif in the Kola Peninsula. Otechestvennaya Geologiya 6, 52-60 [in Russian].

Murashov D.F., 1958. Ultrabasic intrusions of the Serpentinite belt (Pados-Tundra etc.). In: Geology of the USSR, Murmanskaya oblast, Geological Description 27. Gosgeoltekhizdat, Moscow, 318-321 [in Russian].

Nikiforov A.A., 2018. Associations and crystallization trends of chromian spinels in the Pados-Tundra complex, Kola Peninsula. In Actual problems of geology, geophysics and geo-ecology Proceedings of the XXIX conference of young researchers devoted to the memory of K.O. Kratz and F.P. Mitrofanov. Institute of Geology, Karelian Research Centre of the Russian Academy of Sciences (RAS), Petrozavodsk, Russia, 76-79 (in Russian).

Shlayfshteyn B.A., 1987. The account on results of additional geological appraisal at a scale of 1: 200,000 in the northwestern part of the Kola Peninsula (1981-1987 years). The Central-Kola geological survey (expedition), "Sevzapgeologiya", the Ministry of Geology of the RSFSR (in Russian).

Shukevich A.M., 1933. An Account of Geological Mapping in the Rivers Nota and Pecha basin in the years 1932-1933 (Kola Peninsula). The Leningradsky (Northwestern) Geological Survey; inventory number 52 (unpubl. Report; in Russian).

Shukevich A.M., 1936. The Final Account of Field Trips by the Pados-Tundra Geological Party No. 9 (Kola Peninsula). The Leningradsky (Northwestern) Geological Survey; inventory number 96 (unpubl. Report; in Russian).

Sokolova V.N., 1960 (D.V. Palferov, Ed.). Geological Map of Mineral Resources of the USSR (scale 1:200,000; R-36-

XXXI, XXXII): Kola Series, North-Western Geological Department, Ministry of Geology & Mineral Resource Protection of the USSR, Gosgeoltekhizdat, Moscow.

Spirov V.N., 1972 (Principal investigator). Geological map (1:10,000) of the detailed mapping area at River Khlebnaya; an Account of the western Kola geological party for the years 1968-1971. The Allarechensky geological party, North-Western Territorial Geological Department, Murmansk Geological-Prospecting Expedition, the U.S.S.R. Ministry of Geology, Murmansk (unpubl. Map and Report; in Russian).

Staudigel H. and Schreyer W., 1977. The upper thermal stability of clinochlore, $Mg_5Al[AlSi_3O_{10}](OH)_8$, at 10-35 kb P H_2O. Contributions to Mineralogy and Petrology 61, 187-198.

Vinogradov L.A., 1971. The formations of ultrabasic rocks in the southwestern part of the Kola Peninsula (The Notozersky ultrabasic belt). In Problems of Magmatism of the Baltic Shield. Nauka, 147-153 (in Russian).